Optimization-Based Fault Location Algorithm for Series-Compensated Power Transmission Lines

SILVIO GIUSEPPE DI SANTO[ID], **ALVARO DA ROCHA ALBERTINI**[ID], **AND RODRIGO ROZENBLIT TIFERES**[ID]

Laboratório de Pesquisa em Proteção e Automação de Sistemas Elétricos, Universidade de São Paulo, São Paulo 05508-010, Brazil

Corresponding author: Silvio Giuseppe Di Santo (silviogiuseppe@usp.br)

ABSTRACT This paper presents an optimization-based fault location algorithm applicable to series-compensated power transmission lines. The presented method determines the fault location minimizing the errors between measured and calculated post-fault voltage and current phasors through a dynamic differential evolutionary optimization algorithm. This fault location solution may be advantageous over existing approaches found in the literature as it can locate any fault regardless of the series compensation's design, impedance, and positioning. To validate the proposed algorithm, the authors tested it against more than a thousand and six hundred faults on a 500 [kV] series-compensated double-circuit transmission line simulated in ATP/EMTP. The results indicate that the presented method yields accurate fault location estimates, with errors within the 1% magnitude using post-fault steady-state and transient data. In addition, the proposed algorithm is robust even in situations featuring high-resistance faults, errors in the line's parameters, in the system equivalents connected to and between the line's terminals, and in phasor extraction, configuring it as an accurate and reliable alternative to locate faults within series-compensated lines.

INDEX TERMS Fault location, optimization, series-compensated lines.

I. INTRODUCTION

It is usual in conventional power systems design for large power plants to be located afar from load centers due to planning criteria such as land and resource availability, environmental concerns, and many others. Generated electrical power must then be delivered to consumers through lengthy transmission lines able to transfer power over significant distances to consumers spread over the utility service area [1].

As energy demand historically increases, companies have made tremendous efforts to enhance power transmission capabilities while maintaining the necessary stability, safety, and reliability. Thus, the transmission grid is an essential power link, and any interruption of its performance may develop severe outcomes. A need arises for effective methods to protect, recognize, locate, treat, and perform maintenance of faults and events that may occur in the grid.

Several works in the literature have been investigating different techniques to improve the capacity, stability, and performance of power delivery [2]–[6]. Power transmission is related to the transmission lines' reactance and buses voltages. The voltage characteristics must be kept within acceptable safety margins, and therefore they may reach limited ranges. Thus, power transmission enhancement techniques explore influencing lines' apparent reactance.

A widely applied and studied method is inserting a capacitor bank in series with the transmission line [1], [7]. The capacitive reactance connected in series with the line results in an apparent reduction of the inductive reactance, which increases stability margins and power transfer capacity given the assumption of constant voltage magnitudes and angles. Additionally, capacitive series compensation (SC) provides benefits such as improved voltage profiles, enhanced angular stability, and oscillations damping.

Design of SC includes, additionally to the capacitor bank, protective components necessary for safe operation. In general, a bypass switch is used to aid the connection of the compensation to the transmission line, while a spark gap and a metal-oxide varistor (MOV) act as protection against voltage fluctuations [6].

However, while series compensation allows improved power transmission through longer distances and extended capacity, it also challenges fault location algorithms. The protective elements of the series compensation introduce undesirable non-linear behavior to the system. The MOV acts as first protection during events by allowing fault current to instantaneously flow through a low impedance path, resulting in a non-linear behavior as the capacitor bank and MOV conduct current alternatively in each cycle [8].

A. CONTRIBUTION OF THIS WORK

The precise fault location in series-compensated transmission systems is a concern that demands efforts in the development of new methodologies. In general, fault location algorithms may be essentially classified into: phasor-based algorithms [7]–[20], instantaneous time-domain algorithms [21]–[23], and traveling wave (TW) algorithms [24]–[27].

Several phasor-based methods have been developed over the past years to locate faults in series-compensated transmission lines. Generally, these algorithms employ more than one subroutine that search for faults in each path between the terminals and the series compensator. In [13], for instance, there are two subroutines responsible for estimating the fault distance simultaneously, with one of them yielding the correct estimate. The subroutines use the voltage and current phasors obtained from both transmission line's terminals. Although the authors mention that the voltage and current signals may be unsynchronized, synchronization is needed for the proper determination of the fault distance. Another disadvantage is that this algorithm is applied only in cases in which the series compensation is not bypassed during faults, which therefore limits this method's applicability.

The authors of [14] propose an iterative methodology to locate the fault. This algorithm needs prior knowledge of the fault type and the pre-fault data to perform synchronization. Similarly to [13], this method also relies on two fault location subroutines. Another similar technique is presented in [16]. However, it is only applicable in cases where the compensation has been bypassed. Furthermore, for the convergence of the phasor estimation technique, there must be enough time between the instants in which the MOV is bypassed and the protection device actuation. Nevertheless, there are cases in which the protection operates before bypassing the SC.

The method proposed in [8] is only applicable to faults involving ground. Besides, it assumes that the compensators involved in the faulted phases have equal impedance, which may lead to errors when the phases are unbalanced. In the method proposed by [7], in turn, an investigative subroutine is first performed at one side of the compensated line. If a solution is found, the method stops the search. Otherwise, the search continues at the other side. The authors provided no details concerning the phasors estimation. The method proposed by [18] also uses two subroutines and the phasors obtained from the measurements of the two transmission line terminals to locate the fault. However, it requires prior knowledge of the series compensation impedance during the fault and is not applicable for balanced faults.

Differently, the phasor-based method proposed by [19] implements just one subroutine to locate the fault. It applies to a system with three-terminal single-circuit lines. This method divides the system into four sections to locate the fault. Furthermore, for each of these sections, it performs the calculation of all fault types and estimates the correct result based on the system's boundary conditions. A phasor-based method using only current signals from the terminal which contains the compensation is proposed by [20]. The fault location is done in two steps, being the first one responsible for the estimation of the current phasor and the initial fault location and the second one responsible for, through statistical calculations, improving the fault location estimation. However, it is only applicable for phase-to-ground faults.

The authors of [28] presents a method to locate faults on medium voltage distribution feeders, which supply power to residential and commercial consumers. Therefore, despite employing the nodal admittance matrix similarly to this work, it is a solution to distribution networks that deal with the challenges of this type of system. Additionally, differently from this work, this algorithm uses a probabilistic analysis to identify the faulted network's section, once distribution feeders generally present several ramifications and variable load profiles, outcoming in different possible fault points.

In [29], the authors present an algorithm that locates faults in double-circuit compensated lines that employs a six-sequence component transformation to locate any faults accurately. However, the method considers that the SC impedance is known and that it is the same in all faulted phases, which may not always be true due to the compensation's non-linear behavior. The method proposed by [30], on the other hand, locates faults on series compensated transmission lines minimizing the error between the voltages calculated in the fault point from each transmission line terminal. The main disadvantage of this method relies on the necessity of knowing the MOV's non-linear characteristic, and it cannot be employed in Thyristor Controlled Series Compensation (TCSC) compensated lines.

Time-domain algorithms uses directly the measured voltage and current samples to locate faults. These methods are usually limited by the instrument transformers (ITs) characteristics, which may not be able to precisely follow rapid changes and are noise-sensitive [20]. A time domain method using synchronized line terminal voltage and current signals is presented in [23]. However, it demands sampling rates of at least 40 [kHz] and may be affected by noisy measurements.

TW-based algorithms monitor the voltage and current signals moving through the conductors to locate faults. They usually present high precision results. However, they are also very sensitive to noises in the monitored signals and require expensive equipment with high sampling rates. The method

proposed by [25], for instance, uses a wavelet transformation to filter local voltage and current signals captured near the series compensator. The first TW is used to differentiate in which side of the compensation the fault occurs, while the polarity of the second is used to calculate the fault location. The authors of [27], in turn present a TW-based fault locator that uses the first two wave arrival times in each line terminal to accurately locate the fault point. However, it demands a sampling frequency within the [MHz] magnitude and therefore may not be suitable for most commercial device.

Therefore, the main concerns surrounding the fault location in compensated-lines state-of-the-art are the necessity of voltage and current data to include a post-fault period in which the SC was removed by the protection, previous knowledge of MOV and SC characteristics (impedance and operation points), non-applicability to all fault types, and limitations related to the compensator's positioning.

Hence, the contribution of this work is the proposal of a fault location algorithm that addresses all the listed concerns. This method uses current and voltage data acquired from both the line's terminals, and is based on an optimization algorithm that uses Dynamic Differential Optimizer (DDEOPT) to determine the fault location, the fault resistance, and the SC impedances. Additionally, it can locate faults regardless of the series compensation model and positioning. Furthermore, the proposed method does not need to wait for the capacitors bypassing to extract the current and voltage phasors. To the best of the authors' knowledge, there is no similar method that addresses altogether the described concerns.

The authors evaluated the proposed algorithm through its application on more than a thousand six hundred faults simulations in an actual 500 [kV] transmission line in ATP/EMTP. The results indicate that the method can locate any faults accurately, even in critical conditions concerning errors in the phasors extraction and the line's and equivalents' parameters.

B. MANUSCRIPT STRUCTURE

The remaining sections of this paper are organized as follows: sec. II presents the modeling and functions concerning SC of transmission lines. Sec. III, in turn, describes in detail the proposed algorithm's methodology. Sec. IV presents the obtained results and analyses, alongside the simulated compensated line. Also, sec. IV regards the method's performance in cases with errors in phasor extraction, line parameters, and on the equivalents connected to and between the line's terminals. Sec. V, finally, concludes this article.

II. TRANSMISSION LINES SERIES COMPENSATION

The literature displays various kinds of SC designs, from which two main groups stand out: Fixed Series Compensation (FSC) and TCSC. A basic FSC setup includes a series capacitor bank in parallel with protection elements such as over-voltage protection and bypass breaker. An FSC capacitor is not variable, and its rating relates to normal operating conditions (over-sizing may not be economically attractive).

The primary over-voltage protection is a MOV, a highly non-linear element. It serves as a bypass for the capacitor bank during fault occurrence, as it conducts freely whenever the voltage across its terminals is higher than a specific threshold. The remaining breaker in this design is normally open and used to switch the capacitors in or out of operation.

The TCSC employs a similar design but with anti-parallel thyristors controlling an air-core reactor, shunting the series capacitor. The ability to control the thyristors' commutation gives the operational advantage to manage the compensation level, ranging from inductive to capacitive values through the thyristors firing angle. With the development and facilitated power electronics usage, TCSC has become more prominent. The TCSC presents some advantages over the FSC, such as their very fast response time and ability to choose thyristor commutation instants, minimizing transients, and allowing a rapid and continuous control of the compensation. Besides, they present a longer life-cycle due to the reduced number of mechanical switches, inter-area oscillation damping, voltage support, and short-circuit restriction [6].

As the modeling of these elements may vary, different planning and operational challenges arise. Every modeling process introduces more design parameters and, thus, uncertainties that may induce errors and increase processes complexity. Thus, the scientific community has been studying their main challenges and impacts, such as stabilization and transient stability controls, planning studies, protection and fault location issues, and sub-synchronous resonance [6], [31], [32]. An example is the MOV. This non-linear protective element is efficient for the SC protection, as it enables an instantaneous bypass of the capacitors during emergencies. However, it challenges the fault location algorithms, as its impedance is unknown during the fault. Therefore, it has been understood that the ability to design efficient fault location algorithms independent from the MOV model is crucial for the transmission system's planning and operation.

III. METHODOLOGY

The literature review shows that there are several concerns about the fault location in series-compensated transmission lines, such as voltage and current data availability requirements, previous knowledge of MOV and compensation characteristics and limitations to fault types applicability, and series compensation positioning.

Thus, it is evident the necessity of a fault location method that addresses the observed concerns efficiently and precisely. In this way, in this research, the authors propose an algorithm to locate faults within series-compensated lines. The proposed method uses voltage and current data acquired from both transmission line terminals. It is capable of locating faults of any type, regardless of the series compensation model or its position in the transmission line. Additionally, the algorithm does not need to wait for the protection scheme to bypass the series compensation device to initiate the
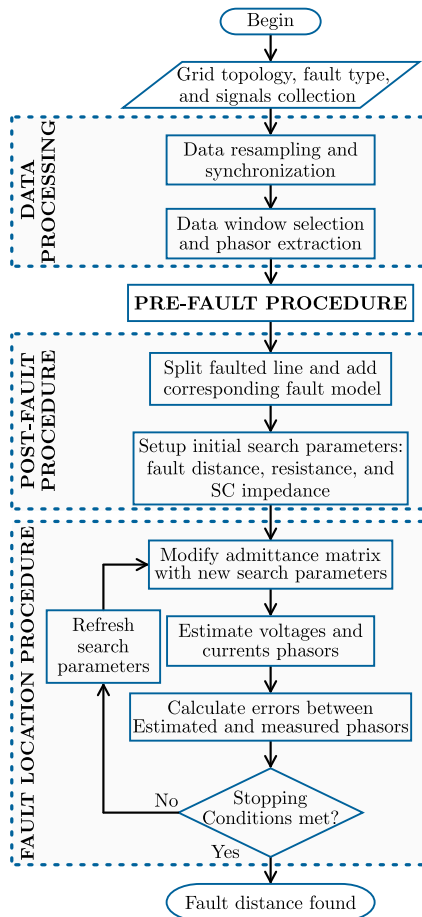
FIGURE 1. Flowchart of the proposed fault location method.

fault location process. The following subsections detail the method's steps, depicted in Fig. 1.

A. DATA PROCESSING

Initially, the voltage and current signals are acquired from the local and remote transmission line terminals. The data processing of the acquired signals includes filtering, synchronization, and phasor extraction steps.

Data filtering should be performed before any subsequent steps of the method. In this way, problems originated by aliasing or spurious noise are mitigated, avoiding fault location errors. The filtered signals synchronization is important to prevent angular errors during phasor estimation. The voltage and current phasors are then extracted from the processed signals for further application in the fault location process.

1) DATA FILTERING AND SYNCHRONIZATION

A digital low-pass Butterworth filter is used for filtering of the signals. The filter design consists of defining frequency and attenuation values for the pass band and for the reject band. Voltage and current signals used in this paper have sampling frequency of 3840 [Hz] or 64 samples per 60 [Hz] cycle. Therefore, the authors selected the values of 90 [Hz]

and 3 [dB] for the cutoff frequency and maximum attenuation of the pass band, respectively. For the cutoff frequency and minimum attenuation of the rejection band, in turn, the authors chose the values of 1920 [Hz] and 40 [dB] respectively. The Nyquist frequency used in this research is 1920 [Hz], which is half of the proposed algorithm's sampling rate.

After filtering, the voltage and current signals from both transmission line terminals must be synchronized. The signals have the same time stamps (provided by the Global Positioning System (GPS)). However, they may have been sampled at different instants. The problem with the lack of synchronization is that a phase error may arise between the phasors obtained from the terminal signals. Thus, the signals are synchronized through an interpolation process.

Another way to synchronize voltage and current phasors between transmission line terminals is to multiply the phasors of one of the terminals by $e^{j\theta}$. The phase θ may be determined by calculating the pre-fault phasors from one terminal using data from the opposite terminal, as proposed by [19]. In more complex grids, an alternative way to determine θ is through a minimization process.

In this research, the authors chose interpolation to achieve the signals synchronization as the pre- and post- fault phasors already have the same time stamps, assigned by the GPS. Still, in the cases whether one or both line terminals have GPS issues, the synchronization method can be adapted to the mentioned minimization-based approach.

2) DATA WINDOW SELECTION AND PHASORS EXTRACTION

Before extracting voltage and current phasors, it is necessary to set the pre- and post-fault data windows, defined by the fault instant, which is known. In case the power or energy absorbed by the MOV reaches its maximum values, during the occurrence of a fault, the series compensation protection device actuates, leading to discontinuity in the signals that may introduce errors in the phasor calculations. Thus, the appropriate selection of the data should consider the longest window delimited by the switching of any SC phases. To perform this task, the authors considers to be known the fault instant and the switching time of the protection in each phase.

Fig. 2 illustrates the three-phase currents of a double phase (b-c) fault alongside the SC protection bypass switching signals and candidate data windows. The currents in phases b and c have distinct amplitudes and are not 180° shifted, which leads to different switching instants. As Window 1 is the largest, the algorithm will choose it. Additionally, as the current amplitudes differ, the impedance at each phase of the SC also changes once the MOV operation is directly proportional to the current magnitude through it. It is noteworthy that if the protection scheme bypasses one of the SC phases in the selected window, the considered impedance is zero.

The phasors extraction algorithm uses both transmission line terminals' synchronized voltage and current selected
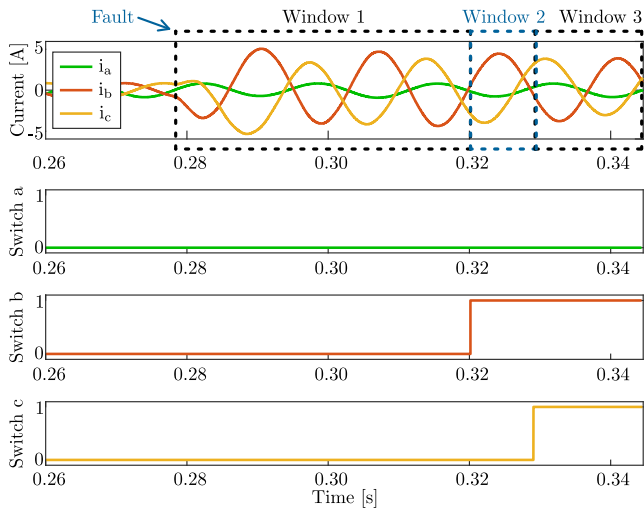
FIGURE 2. Selection of data window for phasor extraction. Instrument current transformer has 3000:1 relation.

data. These signals may contain dc and sub-synchronous components beyond the fundamental and higher-order multiples. Thus, the algorithm must recognize and filter out all components besides the fundamental.

The sub-synchronous components arise from the series compensation capacitance and transmission line inductance interaction. Typically, these components, in addition to the dc exponentially decaying one, appear during faults in series compensated transmission lines. To work with such signals, the authors of [33] have developed an adequate phasor extraction methodology based on the Prony filter together with an Fast Fourier Transform (FFT). Such a signal may be described by (1). In this equation, the terms represent, respectively, the fundamental, the higher-order components, and the transient components (dc and sub-synchronous).

$$s\left(t\right) = a_1 \cos\left(\omega_1 t + \theta_1\right) + \sum_{m=1}^{L} a_m \cos\left(\omega_m t + \theta_m\right)$$
$$+ \sum_{k=1}^{p} b_k e^{\frac{-t}{\tau_k}} \cos\left(\omega_k t + \theta_k\right) \quad (1)$$

where a_1, a_m and b_k are the amplitudes, ω_1, ω_m and ω_k are the angular frequencies, and θ_1, θ_m and θ_k are the phase angles of the fundamental, the higher-order and the transient components. In addition, τ_k is the decaying constant of the transient component, m is the order of the harmonic component, and k is the order of the transient component.

The approach described in [33] is to recognize and filter out the transient components. To determine its properties, i.e. to find out b_k, ω_k, θ_k and τ_k values, the Prony filter is applied to the moving averaged signal [34]. Thus, it is possible to subtract the transient contribution from the original signal. Afterwards, a FFT filter extracts the signal's fundamental term and calculates the phasors.
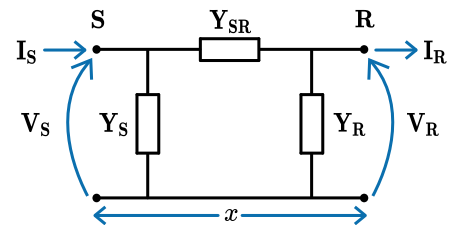

FIGURE 3. Transmission line π-equivalent model.

B. SYSTEM ELEMENTS MODELING
The proposed fault locator uses the grid's nodal equations to locate faults. Hence, the algorithm's precision is linked with the proper modeling of all components. As the components modeling may be somewhat complex, the authors employed the oriented graph theory to perform this task [35].

The theory of oriented graphs allows the physical structure of the electrical grid to be represented in an organized manner, thus avoiding errors in the modeling. The graph theory divides the electrical grid modeling into two parts: one represented by a matrix containing the primitive admittances of the component that compose the electrical grid and the other represented by a matrix, called the incidence matrix, holding the way how these admittances are connected, that is, the topology of the electrical network. Thus, items III-B1 to III-B3 present the modeling of transmission lines, equivalents, SC, shunt reactors, and faults. Item III-D, then, details the grid modeling through the theory of oriented graphs.

1) TRANSMISSION LINE
The transmission line section can be modeled by an π-equivalent circuit, as depicted by Fig. 3. From this circuit one can find the relationships between the voltages and currents at sending (**S**) and receiving (**R**) ends [36], as in (2).

$$\begin{bmatrix} \mathbf{V_S} \\ \mathbf{I_S} \end{bmatrix} = \begin{bmatrix} \mathbf{A}(x) & \mathbf{B}(x) \\ \mathbf{C}(x) & \mathbf{D}(x) \end{bmatrix} \begin{bmatrix} \mathbf{V_R} \\ \mathbf{I_R} \end{bmatrix} \quad (2)$$

where $\mathbf{V_S}$, $\mathbf{V_R}$, $\mathbf{I_S}$, and $\mathbf{I_R}$ are the line terminal voltages and currents in and x is the line's section length.

According to [36], the elements of (2) are described as:

$$\mathbf{A}(x) = \mathbf{y}^{-1}\mathbf{M}\left[\cosh(\gamma_j x)\right]_D \mathbf{M}^{-1}\mathbf{y} \quad (3)$$

$$\mathbf{B}(x) = \mathbf{y}^{-1}\mathbf{M}\left[\gamma_j \sinh(\gamma_j x)\right]_D \mathbf{M}^{-1}\mathbf{y} \quad (4)$$

$$\mathbf{C}(x) = x\mathbf{M}\left[\frac{\sinh(\gamma_j x)}{\gamma_j x}\right]_D \mathbf{M}^{-1}\mathbf{y} \quad (5)$$

$$\mathbf{D}(x) = \mathbf{M}\left[\cosh(\gamma_j x)\right]_D \mathbf{M}^{-1} \quad (6)$$

where $\mathbf{z}$ and $\mathbf{y}$ are the per-unit-length series impedance and shunt admittance matrices, $\mathbf{M}$ the eigenvectors of $\mathbf{yz}$, γ_j is the square root of the eigenvalues of the jth eigenvector of $\mathbf{yz}$, and notation $[\cdot]_D$ indicates a diagonal matrix.

Thus, the admittances of the π-equivalent model may be calculated as shown from (7) to (9), where $\mathbf{I}$ represents the
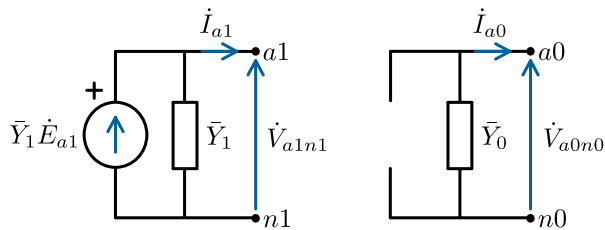
FIGURE 4. Synchronous generator represented in positive (1) and zero (0) sequence components.

identity matrix. These admittances are the transmission line's primitive admittance matrices.

$$\mathbf{Y_S} = [\mathbf{D}(x) - \mathbf{I}] \, \mathbf{B}(x)^{-1} \tag{7}$$

$$\mathbf{Y_{SR}} = \mathbf{B}(x)^{-1} \tag{8}$$

$$\mathbf{Y_R} = \mathbf{B}(x)^{-1} [\mathbf{A}(x) - \mathbf{I}] \tag{9}$$

2) GRID EQUIVALENT

Fig. 4 depicts the circuit of the grid equivalents, represented as a current source in parallel with an admittance. Based on this circuit, the mathematical modeling of the grid equivalent, in phase components, is given as in (10).

$$\begin{bmatrix} \dot{I}_a \\ \dot{I}_b \\ \dot{I}_c \end{bmatrix} = -\mathbf{Y_G} \begin{bmatrix} \dot{V}_{an} \\ \dot{V}_{bn} \\ \dot{V}_{cn} \end{bmatrix} + \mathbf{T} \begin{bmatrix} 0 \\ \bar{Y}_1 \dot{E}_{a1} \\ 0 \end{bmatrix} \tag{10}$$

where $\dot{V}_{an}$, $\dot{V}_{bn}$, $\dot{V}_{cn}$, $\dot{I}_a$, $\dot{I}_b$, and $\dot{I}_c$ are the phase voltages and currents at the equivalent's terminal, $\mathbf{T}$ is the symmetrical components transformation matrix, $\bar{Y}_0$ and $\bar{Y}_1$ are the zero and positive sequence admittances, and $\dot{E}_{a1}$ is the positive sequence internal equivalent voltage. The equivalent's primitive admittance matrix is given as in (11). In addition, equivalents between the line's terminals (transfer equivalent) are modeled as just an admittance.

$$\mathbf{Y_G} = \mathbf{T} \begin{bmatrix} \bar{Y}_0 & 0 & 0 \\ 0 & \bar{Y}_1 & 0 \\ 0 & 0 & \bar{Y}_1 \end{bmatrix} \mathbf{T^{-1}} \tag{11}$$

3) SERIES COMPENSATION

The SC is modeled as a single three-phase impedance [37]. The primitive admittance matrix, as indicated in (12), is constructed by taking the inverse of each phase's impedance.

$$\mathbf{Y_C} = \begin{bmatrix} 1/\bar{Z}_a & 0 & 0 \\ 0 & 1/\bar{Z}_b & 0 \\ 0 & 0 & 1/\bar{Z}_c \end{bmatrix} \tag{12}$$

It is noteworthy that the SC modeling is independent from the compensator's design. The values of $\bar{Z}_a$, $\bar{Z}_b$ and $\bar{Z}_c$ may be different, depending on the MOV operation point and on the bypass of the specific phases. In this case, the impedances goes to zero. As a computational limit, the authors adopted the minimum impedance magnitude value as 10^{-6} to avoid rank-deficient matrices.
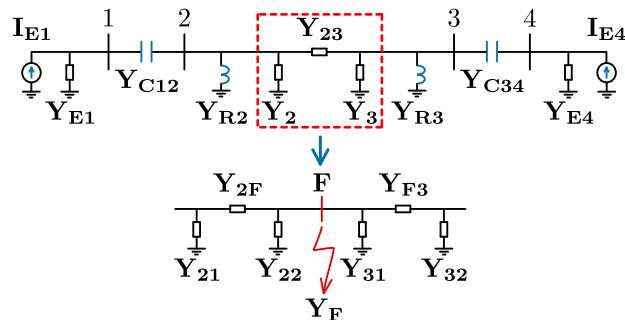

FIGURE 5. Substitution of the pre-fault line for the post-fault sections with the new fault node F in generic electric grid.

4) SHUNT REACTOR

The primitive admittance matrix of the shunt reactor is similar to the series compensator's one, as in (13).

$$\mathbf{Y_R} = \begin{bmatrix} 1/\bar{Z}_a & 0 & 0 \\ 0 & 1/\bar{Z}_b & 0 \\ 0 & 0 & 1/\bar{Z}_c \end{bmatrix} \tag{13}$$

5) FAULT MODEL

The primitive admittance matrix of a generic fault is detailed in (14). This modeling allows the construction of different fault types by setting the necessary admittance values as null. The fault types are phase-to-ground, phase-phase-to-ground, phase-to-phase, and three-phase.

$$\mathbf{Y_F} = \begin{bmatrix} \bar{Y}_a - \bar{Y}_a^2/\bar{Y}_t & -\bar{Y}_a\bar{Y}_b/\bar{Y}_t & -\bar{Y}_a\bar{Y}_c/\bar{Y}_t \\ -\bar{Y}_b\bar{Y}_a/\bar{Y}_t & \bar{Y}_b - \bar{Y}_b^2/\bar{Y}_t & -\bar{Y}_b\bar{Y}_c/\bar{Y}_t \\ -\bar{Y}_c\bar{Y}_a/\bar{Y}_t & -\bar{Y}_c\bar{Y}_b/\bar{Y}_t & \bar{Y}_c - \bar{Y}_c^2/\bar{Y}_t \end{bmatrix} \tag{14}$$

where, $\bar{Y}_t = \bar{Y}_a + \bar{Y}_b + \bar{Y}_c + \bar{Y}_n$.

C. PRE-FAULT PROCEDURE

Fig. 5 depicts a generic electric grid with series and shunt compensations at both line ends, in the pre-fault condition. The proposed method uses the oriented graphs theory to build the nodal equations of electric grids. With the voltage and current phasors at the line ends, and assuming known the admittances of equivalents $\mathbf{Y_{E1}}$ and $\mathbf{Y_{E4}}$, it is possible to determine the equivalent's currents $\mathbf{I_{E1}}$ and $\mathbf{I_{E4}}$, which maintain their values for the post-fault condition and are used by the algorithm in the post-fault modeling.

D. POST-FAULT PROCEDURE

The chosen line for the fault location is divided into two π-sections, with lengths d and $\ell - d$, respectively. Between the sections, the algorithm creates a new fictional node $\mathbf{F}$, as also shown in Fig. 5. The admittances of the new π-section models are given through (7)-(9) with the initially considered lengths. This generalization allows the fault modeling at this node, according to (14), adapted to the occurred fault type.

The method creates the post-fault incidence and primitive admittance matrices through (15) and (16). This allows the assembly of the bus admittance matrix as in (17), used by the

algorithm to solve the nodal equations denoted by (18), which yields the calculated post-fault nodal voltages $\mathbf{V}_1^{(c)}$ and $\mathbf{V}_4^{(c)}$ at the transmission line ends. With currents $\mathbf{I}_{E1}$ and $\mathbf{I}_{E4}$, together the known admittances $\mathbf{Y}_{E1}$ and $\mathbf{Y}_{E4}$, the post-fault calculated currents $\mathbf{I}_1^{(c)}$ and $\mathbf{I}_4^{(c)}$ at the line's ends are given by (19) and (20). For double-circuit lines, the proposed algorithm applied the same methodology, but considers the parallel circuit's admittances and the mutual admittances between circuits, as in (3) to (6).

It is noteworthy that in compensated lines in which the compensation is placed along the line, the proposed algorithm searches for the fault in both line sections comprised between the terminals and the compensator and compares the obtained results to determine the faulted section.

$$
\mathbf{Q} = \begin{array}{c} \\ \mathbf{Y}_{E1} \\ \mathbf{Y}_{C12} \\ \vdots \\ \mathbf{Y}_{F3} \\ \vdots \\ \mathbf{Y}_{C34} \\ \mathbf{Y}_{E4} \end{array}
\begin{array}{c} 1 \ \ 2 \ \ 3 \ \ 4 \ \ F \end{array}
\begin{bmatrix}
\mathbf{I} & \mathbf{0} & \mathbf{0} & \mathbf{0} & \mathbf{0} \\
\mathbf{I} & -\mathbf{I} & \mathbf{0} & \mathbf{0} & \mathbf{0} \\
\vdots & \vdots & \vdots & \vdots & \vdots \\
\mathbf{0} & \mathbf{0} & \mathbf{I} & \mathbf{0} & -\mathbf{I} \\
\vdots & \vdots & \vdots & \vdots & \vdots \\
\mathbf{0} & \mathbf{0} & -\mathbf{I} & \mathbf{I} & \mathbf{0} \\
\mathbf{0} & \mathbf{0} & \mathbf{0} & \mathbf{I} & \mathbf{0}
\end{bmatrix} \quad (15)
$$

$$
\mathbf{Y}_{pr} = \begin{bmatrix}
\mathbf{Y}_{E1} & \mathbf{0} & \cdots & \cdots & \cdots & \mathbf{0} \\
\mathbf{0} & \ddots & \ddots & & & \vdots \\
\vdots & \ddots & \mathbf{Y}_{22} & \ddots & & \vdots \\
\vdots & & \ddots & \mathbf{Y}_{F3} & \ddots & \vdots \\
\vdots & & & \ddots & \ddots & \mathbf{0} \\
\mathbf{0} & \cdots & \cdots & \cdots & \mathbf{0} & \mathbf{Y}_{E4}
\end{bmatrix} \quad (16)
$$

$$
\mathbf{Y}_{bus} = \mathbf{Q}^{\mathsf{T}} \mathbf{Y}_{pr} \mathbf{Q} \quad (17)
$$

$$
\mathbf{Y}_{bus} \begin{bmatrix} \mathbf{V}_1^{(c)} \\ \mathbf{V}_2^{(c)} \\ \mathbf{V}_3^{(c)} \\ \mathbf{V}_4^{(c)} \\ \mathbf{V}_F^{(c)} \end{bmatrix} = \begin{bmatrix} \mathbf{I}_{E1} \\ \mathbf{0} \\ \mathbf{0} \\ \mathbf{I}_{E4} \\ \mathbf{0} \\ \mathbf{0} \end{bmatrix} \quad (18)
$$

$$
\mathbf{I}_1^{(c)} = \mathbf{I}_{E1} - \mathbf{Y}_{E1} \mathbf{V}_1^{(c)} \quad (19)
$$

$$
\mathbf{I}_4^{(c)} = \mathbf{I}_{E4} - \mathbf{Y}_{E4} \mathbf{V}_4^{(c)} \quad (20)
$$

E. FAULT LOCATION PROCEDURE

To locate the fault, the method solves the minimization problem stated in (21). The algorithm seeks to minimize the objective function given by the errors between the calculated and measured post-fault voltage and current phasors quantities. The proposed method requires as inputs: the fault type, the faulted line's length ℓ, and the post-fault measured and calculated terminal voltage and current phasors, denoted with the operators $.^{(m)}$ and $.^{(c)}$, respectively.

$$
\text{Minimize} \quad \varepsilon \left(d, r_{ph}, r_g, \bar{z}_{Ca}, \bar{z}_{Cb}, \bar{z}_{Cc} \right),
$$

$$
\text{subject to} \begin{cases}
10^{-6} \leq d/\ell \leq 1 \\
10^{-6} \leq r_{ph}, \ r_g \leq 1 \\
10^{-6} \leq \Re\{\bar{z}_{Ca}, \bar{z}_{Cb}, \bar{z}_{Cc}\} \leq 1 \\
10^{-6} \leq \Im\{\bar{z}_{Ca}, \bar{z}_{Cb}, \bar{z}_{Cc}\} \leq 1
\end{cases} \quad (21)
$$

The goal of the method is to find fault distance d from the local end of the transmission line, as well as the fault resistances (r_{ph} between phase and neutral, and r_g between neutral and ground), and the phase impedances of the series compensators $\bar{z}_{Ca}$, $\bar{z}_{Cb}$, and $\bar{z}_{Cc}$. All the objective search parameters are calculated by the presented solution as fractions of their corresponding maximum threshold values: fault distance: ℓ, fault resistances: 1000 [Ω], and SC impedances: the rated capacitive reactance.

In the beginning, the objective parameters are guessed within their threshold values. Then, the method divides the measured and calculated terminal voltage and current phasors by their respective largest absolute values, resulting in $\mathbf{v}_1^{(m)}$, $\mathbf{v}_1^{(c)}$, $\mathbf{v}_4^{(m)}$, $\mathbf{v}_4^{(c)}$, $\mathbf{i}_1^{(m)}$, $\mathbf{i}_1^{(c)}$, $\mathbf{i}_4^{(m)}$, and $\mathbf{i}_4^{(c)}$.

Then, the method minimizes the error ε, given by (22), where $\Re.$ and $\Im.$ represent, respectively, the real and imaginary parts of the phasors and $\dot{v}$, i represents their phase $p = \{a, b, c\}$ quantities. The minimal error yields the optimized values for the search parameters, among which is the best approximation for the fault distance d.

$$
\varepsilon \left(d, r_{ph}, r_g, \bar{z}_{Ca}, \bar{z}_{Cb}, \bar{z}_{Cc} \right)
$$
$$
= \Re \left\{ \sum_{n=\{1,4\}} \sum_{p=\{a,b,c\}} \left(\dot{v}_{n,p}^{(m)} - \dot{v}_{n,p}^{(c)} \right) \right\}
$$
$$
+ \Im \left\{ \sum_{n=\{1,4\}} \sum_{p=\{a,b,c\}} \left(\dot{v}_{n,p}^{(m)} - \dot{v}_{n,p}^{(c)} \right) \right\}
$$
$$
+ \Re \left\{ \sum_{n=\{1,4\}} \sum_{p=\{a,b,c\}} \left(i_{n,p}^{(m)} - i_{n,p}^{(c)} \right) \right\}
$$
$$
+ \Im \left\{ \sum_{n=\{1,4\}} \sum_{p=\{a,b,c\}} \left(i_{n,p}^{(m)} - i_{n,p}^{(c)} \right) \right\} \quad (22)
$$

F. OPTIMIZATION FUNCTION

The proposed algorithm uses the DDEOPT, based on differential evolution [38], [39], to minimize the objective function (22). As the genetic algorithm, the DDEOPT algorithm is a population-based method, where through crossover, mutation, and selection processes, more evolved populations are created in each generation. However, this algorithm differs from the traditional genetic algorithm by applying an approach that uses the difference between individuals and presents higher robustness and efficiency [39].

According to [38], algorithm DDEOPT, compared to Pattern Search and Simulated Annealing algorithms, proved superior in minimizing non-linear and non-differentiable functions. Still, in [40], the Genetic Algorithms proved to be even equal or inferior to the Simulated Annealing algorithms.

Furthermore, according to [38], algorithm DDEOPT is robust, practical to use, and quick to converge.

At each iteration, the algorithm determines the calculated terminal voltage and current phasors through (15) - (20) using a set of search parameters, which were guessed in the first iteration. Together with the measured phasors, the method evaluates the error through (22). If any stopping conditions are met, the algorithm ends the optimization process and returns the optimized value of the fault distance. Otherwise, the optimizer considers a new set of values for the search parameters and the process repeats. The stopping conditions are: maximum iterations as 1000 minimum; absolute value of error variation between consecutive iterations as 10^{-7}.

IV. RESULTS

This section presents the results of testing the proposed algorithm against faults simulated in a 500 [kV] series compensated line. The authors varied the fault type, resistance, distance, and inception instant, generating over 1600 different scenarios. The method was tested in all cases with the voltage and current signals arising from the simulations, considering both post-fault steady-state and transient measurements. Furthermore, the authors evaluated the algorithm's performance in situations containing errors on the estimated line's parameters, grid equivalent, and estimated phasors.

A. MODELED SYSTEM DESCRIPTION

Fig. 6 depicts the 500 [kV] and 60 [Hz] series compensated double-circuit transmission line modeled in ATP/EMTP by the authors for the fault simulations. This line has $\ell = 256$ [km] length and features both SCs and shunt reactors (SRs) at its terminals. This line's local end (L) is located in Brazil's Center-West region, while the remote end (R) is in the North.

In addition to the SCs and SRs, Fig. 6 also generically illustrates the ITs housed in the respective substations: current transformers (CTs) with 3000:1 ratio, capacitive voltage transformers (CVTs) with 500 [kV] to 115 [V] decrease ratio, circuit breakers (CBs), and intelligent electronic devices (IEDs) that embed the presented fault location solution.

The equivalent at L has $Z_{0L} = (0.6672 + j14.07)$ [Ω], $Z_{1L} = (0.9518 + j18.50)$ [Ω], and $575\angle40°$ [kV] voltage. The equivalent at R, in turn, has $Z_{0R} = (17.43 + j79.71)$ [Ω], $Z_{1R} = (2.9256 + j21.82)$ [Ω], and $556.5\angle-13°$ [kV] voltage. The transfer equivalent between the line's terminals, finally, has its impedance values equal to $Z_{0T} = (340.7 + j749.7)$ [Ω] and $Z_{1T} = (6.438 + j36.40)$ [Ω].

The SRs at both terminals and in both circuits have a rated reactive power of 59 [MVAr]. The authors modeled the SCs according to actual the device operating on this line, illustrated in Fig. 7. All faults were simulated in circuit 1.

B. SIMULATIONS SETUP

The authors used the generic fault model displayed by Fig. 8 in the simulations. The fault scenarios included, for each fault type, the following value combinations for the
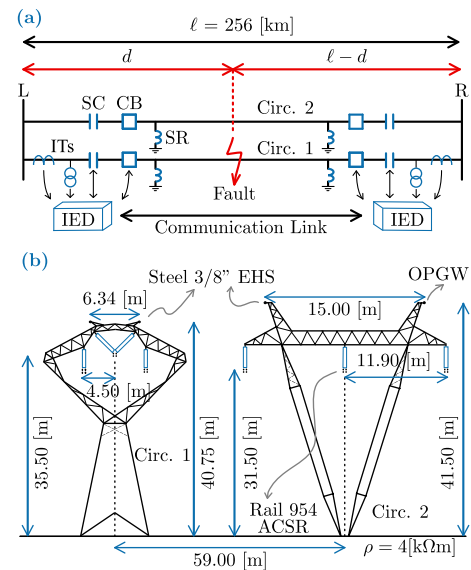

FIGURE 6. Modeled and simulated double-circuit 500 [kV] transmission line with fault location and protection apparatus (a) and towers layout (b).
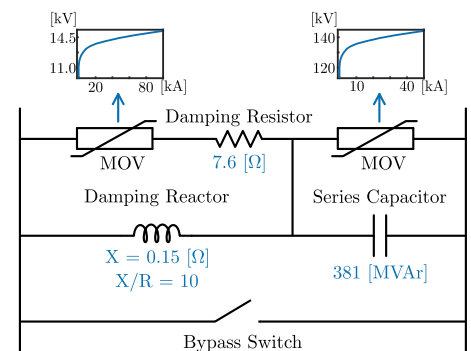

FIGURE 7. Modeled line's SC and MOVs characteristics.

phase (R_{ph}) and ground (R_g) fault resistances respectively: 1 (0.1;0.1), 2 (5;0.1), 3 (10;0.1), 4 (0.1;50), 5 (5;50), 6 (10;50), 7 (0.1;150), 8 (5;150), 9 (10;150), 10 (0.1;500), 11 (5;500), and 12 (10;500) [Ω].

The faults were applied at $d = 0.02, 0.10, 0.30, 0.50, 0.70, 0.90,$ and 0.98 [pu] of the line's length from terminal L, at inception instants 0.2791 and 0.2833 [s], which respectively led to the minor and major dc components in the signals. Four post-fault cycles were simulated for each fault.

Items IV-C and IV-D present, respectively, the results of the methodology's precision and sensitivity to errors in the estimated phasors, transmission line parameters, and terminals' equivalents. All analysis were performed by taking fault scenarios from the aforementioned configurations.

The authors conducted the precision analyses for fault distance variations, considering all resistance combinations for each fault distance and type, and determining the mean and standard deviation. Besides, the authors also performed the analyses for fault resistance variations where, for each
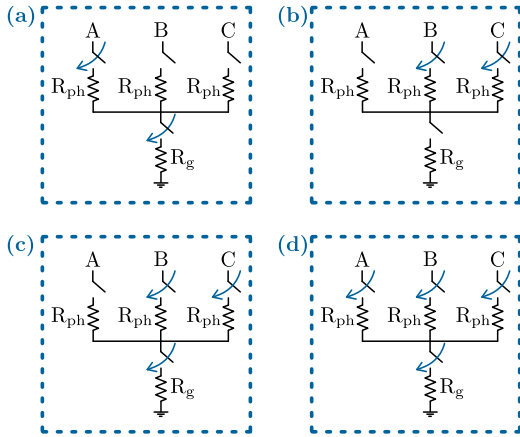
FIGURE 8. Model to simulate phase A to ground (AG) faults (a), phase B to phase C (BC) faults (b), phase B to phase C to ground (BCG) faults (c), and phase A to phase B to phase C to ground (ABCG) faults (d).
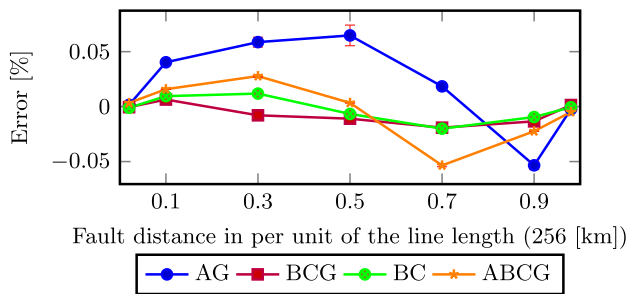

FIGURE 9. Fault distance mean errors for distance variations, with phasors extracted from steady-state.

FIGURE 10. Fault distance mean errors for fault resistance variations, with phasors extracted from steady-state.

TABLE 1. Statistic summary of fault distance errors (%) using phasors extracted from steady-state measurements.

Fault type	Mean error	Standard deviation	25th percentile	Median	75th percentile
AG	0.0183	0.0875	-0.0205	0.0060	0.0505
BCG	-0.0063	0.0256	-0.0165	-0.0020	0.0065
BC	-0.0024	0.0234	-0.0125	-0.0010	0.0110
ABCG	-0.0044	0.0344	-0.0255	-0.0045	0.0130

fault resistance combination and type, all fault distances were considered in the mean and standard deviation calculations.

The sensitivity analysis about errors in the phasors was performed by adding to them a random error phasor of magnitude with 0.5% mean and 0.25% standard deviation, referred to the phasor magnitude, with phase ranging randomly from $-180°$ to $+180°$ [41]. The authors conducted the sensitivity analysis about errors in the transmission line's parameters and errors in the terminal's equivalents by applying, in both studies, errors with normal distribution having zero mean and standard deviation of $\pm5\%$. In the three sensitivity analyses, the authors considered all faults types, at 50% from the L terminal, and fault resistance combination 5 (5;50).

C. PRECISION ANALYSIS
1) FAULT DISTANCE VARIATION
Fig. 9 presents, for each fault type, the fault distance mean errors considering various fault locations, with phasors extracted from steady-state data. The largest error was $0.065\% \pm 0.145\%$, for an AG fault at 50% from L.

Additionally, the authors computed results for cases where the phasors were extracted from the transient period. Considering the fault inception at 0.2791 [s], the most significant mean error was $0.199\% \pm 0.155\%$ for an ABCG
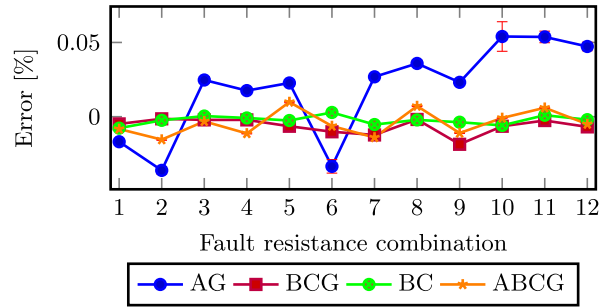
fault at 10% from the L. For faults with start at 0.2833 [s], the largest mean error was $0.451\% \pm 0.138\%$ for an AG fault at 50% from L.

2) FAULT RESISTANCE VARIATION
Fig. 10 presents, for each fault type, the fault distance mean errors considering various fault resistances, with voltage and current phasors extracted from steady-state. The most significant mean error was $0.054\% \pm 0.184\%$ for an AG fault with fault resistance combination 10 (0.1;500). Additionally, the authors computed results of cases in which the phasors were extracted from transient measurements. The most significant mean error was $0.237\% \pm 0.300\%$ for an AG fault with resistance combination 3 (10;0.1) and fault instant at 0.2791 [s]. For the faults with start instants of 0.2833 [s], the most significant mean error was $0.377\% \pm 0.421\%$ for an AG fault with fault resistance combination 12 (10;500).

3) FURTHER DISCUSSION ON PRECISION ANALYSIS
In addition to the results obtained in items IV-C1 and IV-C2, Tab. 1, Tab. 2, and Tab. 3 present the fault location errors statistic summaries considering phasors extracted respectively from steady-state (considering both fault inception instants), transient fault measurements from faults with start instant of 0.2791 [s], which led to the minor dc decaying component, and with start instant 0.2833 [s], which led to the major dc decaying component.

In absolute terms, the largest error obtained was 0.451%, occurred for an AG fault at 50% from L terminal with fault resistance combination 10 (0.1;500). For phasors extracted

TABLE 2. Statistic summary of fault distance errors (%) using phasors extracted from transient measurements (fault inception instant of 0.2791 [s]).

Fault type	Mean error	Standard deviation	25th percentile	Median	75th percentile
AG	0.0281	0.4078	-0.2090	0.0615	0.2695
BCG	0.0781	0.2004	-0.0490	0.0620	0.1625
BC	0.0661	0.1693	-0.0410	0.0310	0.1285
ABCG	0.0873	0.1615	0.0010	0.0705	0.1780

TABLE 3. Statistic summary of fault distance errors (%) using phasors extracted from transient measurements (fault inception instant of 0.2833 [s]).

Fault type	Mean error	Standard deviation	25th percentile	Median	75th percentile
AG	0.1309	0.3566	-0.0995	0.0525	0.3730
BCG	0.1317	0.2266	0.0175	0.0685	0.2450
BC	0.1380	0.2248	0.0115	0.0725	0.2180
ABCG	0.1046	0.1394	0.0235	0.0645	0.1520
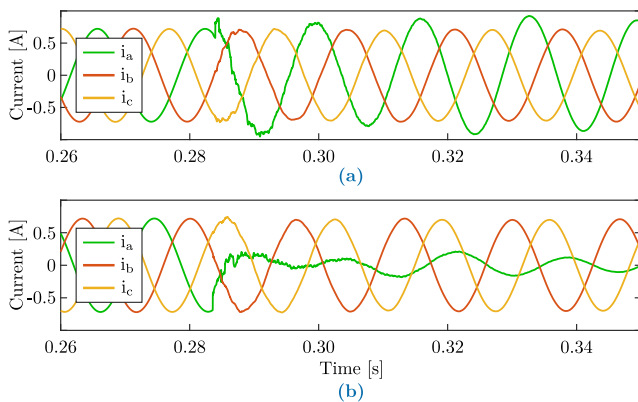
FIGURE 11. Currents in terminal L (a) and R (b) for the AG fault that yielded the most significant location error with phasors extracted from the transient period (1.019%).

from the transient period, with fault instant at 0.2791 [s], the most significant error was 1.002% for an AG fault at 70% from L terminal with fault resistance combination 7 (0.1;150). Finally, for phasors extracted from the transient period, but with fault instant at 0.2833 [s], the most significant error was 1.019% for an AG fault at 70% from L terminal with fault resistance combination 9 (10;150). Fig. 11 depicts, in this way, the line terminals' of this fault.

Another point worth mentioning is the characteristic of the most significant errors. They occurred for AG faults with high resistance values between 50% and 70% of the transmission line's length. Despite that, the presented method's maximum fault location errors were 0.451% (for phasors extracted from steady-state measurements) and 1.019% (for phasors

TABLE 4. Maximum errors obtained by other algorithms found in the recent literature. Maximum errors of the proposed method were 0.451% (phasors extracted from steady-state data) and 1.019% (phasors extracted from transient data).

Reference	Maximum error (%)	Observations
[8]	1.45	Method is only applicable to locate ground faults
[27]	0.37	Method requires sampling frequency of at least 500 [kHz]
[29]	1.86	Method requires the series series compensator's impedance
[30]	0.95	Method requires the MOV's non-linear characteristic

extracted during transient measurements), indicating the method's accuracy and efficiency.

The authors compared these maximum errors with the maximum errors obtained by other algorithms proposed in recent works found in the literature, as illustrated in Tab. 4. One can notice that the proposed solution's maximum errors are similar to the other approaches' maximum errors. Still, these approaches present the drawbacks mentioned earlier, in Sec. I-A.

D. SENSITIVITY ANALYSIS
The authors performed the sensitivity analysis by testing the method's robustness against errors in voltage and current phasors, in the line's parameters, and on the equivalents at and between the line terminals.

1) VOLTAGE AND CURRENT PHASORS ERRORS
Fig. 12 presents the results for the sensitivity analysis regarding errors in the phasors. The authors performed a statistical analysis and constructed a histogram, normalized in probability density, for each fault type, altogether with a probability density curve, and a results box diagram.

Observing Fig. 12 and Tab. 5, one can note that the largest mean error occurred for ABCG faults, while the lowest for BCG faults. For ABCG faults, the mean error was $-0.2254\% \pm 0.7076\%$, with the 25th percentile at -0.7438% and the 75th percentile at 0.3885%. Thus, an ABCG fault distance estimation with errors in the phasors has a 50% of probability to lie between these errors. Besides, the inferior and superior errors were equal to -1.5622% and 1.1149%.

For BCG faults, the mean error was $-0.0068\% \pm 0.2014\%$, with the 25th percentile at -0.1519% and the 75th percentile at 0.1347%. Therefore, a BCG fault distance estimation with errors in the phasors has a 50% probability of lying between such errors. In addition, the inferior and superior errors were respectively equal to -0.3570% and 0.3315%.

2) ERRORS IN THE LINE's PARAMETERS
Fig. 13 presents the results obtained for the sensitivity analysis of errors in the transmission line's parameters. Thus, as in IV-D1, a statistical analysis was performed.

TABLE 5. Fault distance errors in (%) considering deviations on phasors, parameters, and equivalents. Faults at 50% (128 [km]) from L terminal, resistance combination 5 (5;50), and phasors extracted from steady-state.

Errors on	Fault type	Mean error	Standard deviation	25th percentile	Median	75th percentile
Phasors	**AG**	-0.1043	0.5994	-0.5193	-0.1363	0.2438
	BCG	-0.0068	0.2014	-0.1519	0.0073	0.1347
	BC	-0.0268	0.2281	-0.1488	-0.0321	0.1508
	ABCG	-0.2254	0.7076	-0.7438	-0.1524	0.3885
Parameters	**AG**	-0.6423	2.0866	-1.6435	-0.5771	0.7942
	BCG	-0.0377	2.1834	-1.7197	0.3227	1.1457
	BC	-0.8854	2.1056	-2.6003	-1.1202	0.4358
	ABCG	0.2926	2.6384	-2.0547	-0.6935	2.4866
Equivalents	**AG**	-0.0490	0.1993	-0.1938	-0.0382	0.0818
	BCG	-0.0314	0.0316	-0.0576	-0.0326	-0.0084
	BC	-0.0232	0.0400	-0.0502	-0.0285	0.0009
	ABCG	-0.4259	0.2555	-0.6581	-0.4595	-0.2051

Hence, observing Fig. 13 and Tab. 5, one can note that the most significant mean error occurred for BC faults, while the lowest errors occurred for BCG faults. The mean error was $-0.8854\% \pm 2.1056\%$ for BC faults, with the 25th percentile at -2.6003% and the 75th percentile at 0.4358%. In this way, a BC fault distance estimation with line parameter errors has a 50% probability of lying between these errors. Also, the inferior and superior errors were -4.6281% and 3.4725%.

The mean error was $-0.0377\% \pm 2.1834\%$ for BCG faults, with the 25th percentile at -1.7197% and the 75th percentile at 1.1457%. Hence, a BCG fault distance estimation with errors in the line's parameters has a 50% of lying between these errors. In addition, the inferior and superior errors were respectively equal to -4.0961% and 4.3183%.

3) ERRORS IN EQUIVALENTS AT AND BETWEEN TERMINALS
Fig. 14 presents the results obtained in the sensitivity analysis regarding errors in the equivalents connected to the transmission line's terminals and between them (transfer equivalent). As previously, a statistical analysis was performed.

Observing Fig. 14 and Tab. 5, one can note that the largest mean error occurred for ABCG faults and the lowest mean error occurred for BC faults. For ABCG faults, the mean error was $-0.4259\% \pm 0.2555\%$, with the 25th percentile at -0.6581% and the 75th percentile at -0.2051%. In this way, an ABCG fault distance estimation with errors in the equivalents has a 50% chance of lying between these errors. The inferior and superior errors were -0.8839% and -0.0064%.

For BC faults, in turn, the mean error was $-0.0232\% \pm 0.0400\%$, with the 25th percentile at -0.0502% and the 75th percentile at 0.0009%. Therefore, a BC fault distance estimation with errors in the equivalents has a 50% probability of lying between such errors. Furthermore, the inferior and superior errors were -0.1046% and 0.0720%.
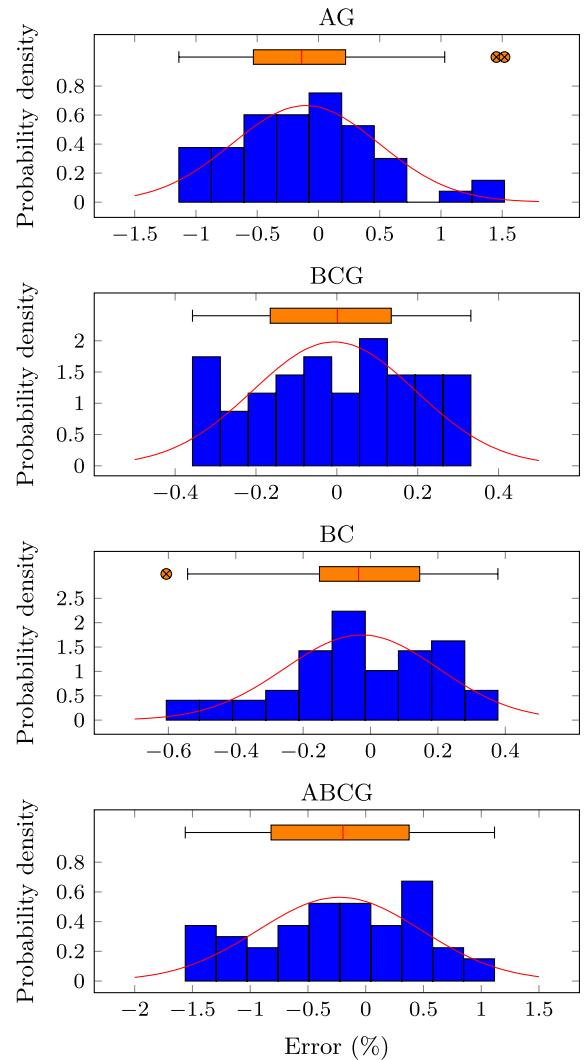

FIGURE 12. Fault location errors with deviations on voltage and current phasors for all fault types. Faults at 50% (128 [km]) from L terminal, resistance combination 5 (5;50), and phasors extracted from steady-state.

4) FURTHER DISCUSSION ON SENSITIVITY ANALYSIS
The analyses presented in IV-D1 to IV-D3 show the proposed algorithm's robustness to locate faults accurately, even in cases with deviation on phasors, parameters, and equivalents.

The authors deliberately applied errors to all voltage and current phasors, leading to more significant fault distance estimation errors than applying errors to a single phasor quantity. The most significant error occurred for an AG fault (1.5185%), which was treated by the statistical analysis as an outlier. However, the mean errors stayed between -0.0068% (BC faults) and -0.2254% (ABCG faults), indicating the method's robustness against errors in phasor estimation.

The errors followed the level of displacement applied to the parameters, which were ±5%, considering deviations in the line's parameters. This behavior occurs due to the apparent lengthening or shortening of the line. However, in actual lines, the positive sequence parameters have greater precision as
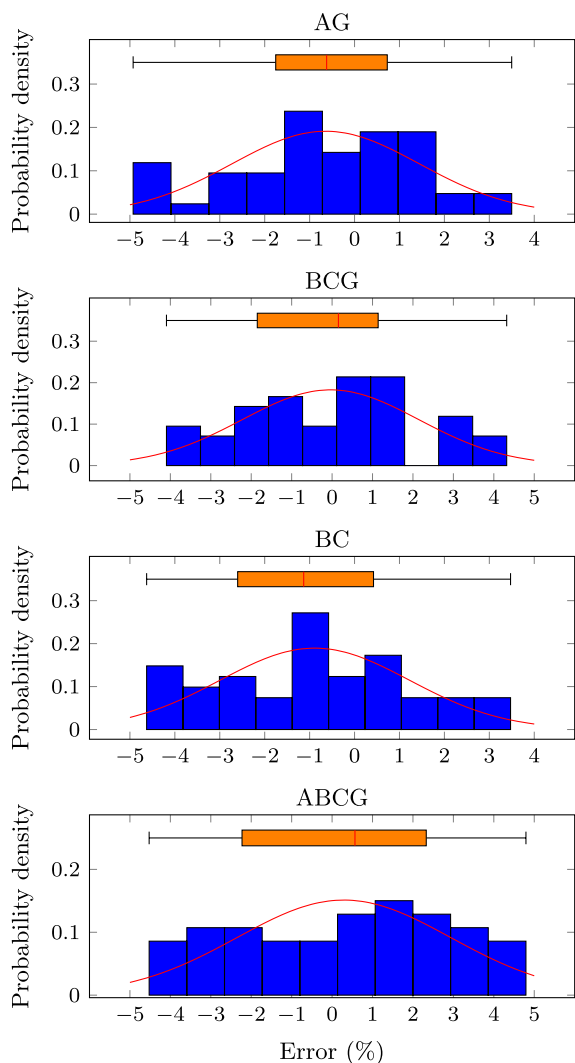
FIGURE 13. Fault distance errors considering deviations on transmission line parameters for all fault types. Faults at 50% (128 [km]) from L terminal, resistance combination 5 (5;50), and phasors extracted from steady-state.

FIGURE 14. Fault distance errors considering deviations on equivalents for all fault types. Faults at 50% (128 [km]) from L terminal, resistance combination 5 (5;50), and phasors extracted from steady-state.

they are independent of the soil resistivity, whose value may vary along the line. Thus, the estimation of the zero-sequence parameters generally is more error-prone. The deviations in the equivalents were more significant for ABCG faults, reaching -0.8839%, considerably distant from the deviation range adopted ($\pm 5\%$). Therefore, according to the results, the method is robust and efficient even under deviations in phasors, parameters, and equivalents, turning out to be a valuable tool for O&M utilities' operators.

E. OPTIMIZATION ANALYSIS

The authors applied different optimization solvers using MATLAB$^{©}$ to the proposed methodology in order to evaluate the impacts on the fault location procedure. Four optimization methods were chosen for this analysis, being: Dynamic Differential Optimizer (DDEOPT), Pattern Search (PS), Simulated Annealing (SA) and Genetic Algorithm (GA).
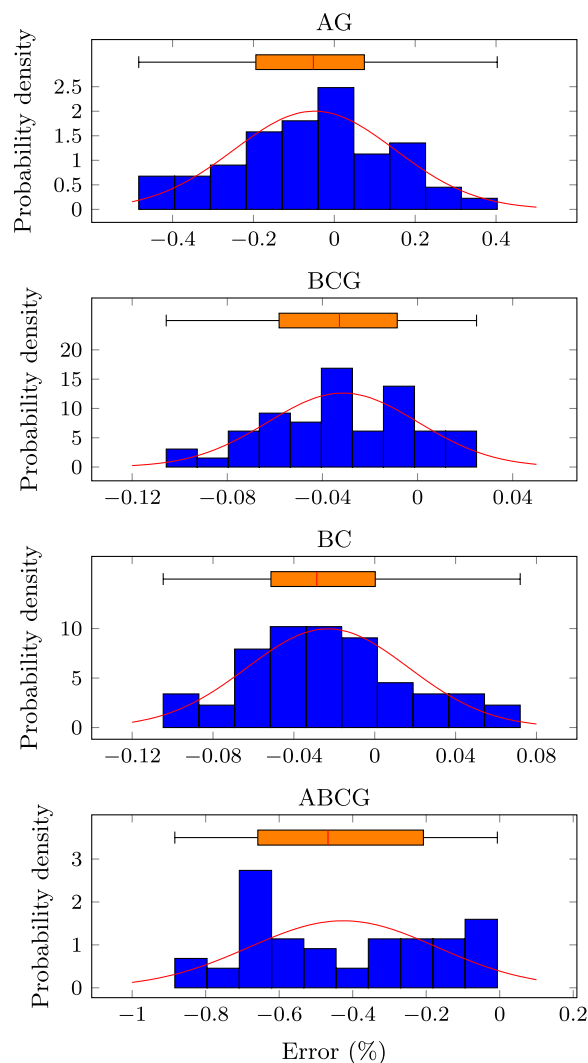
The DDEOPT and the GA solvers were configured with a population size of 50 and 800 maximum generations, being the stopping criteria 10^{-6} for both of them. A 0.8 crossover probability and stepsize was used in DDEOPT. The selection function for the GA was stochastic uniform with constraint dependent mutations. PS configurations were a complete poll analysis using method *MADS Positive Basis 2N* with a mesh tolerance of 2^{-11}. As for the SA, the temperature update used the exponential function with a 3000 maximum function evaluations and a 10^{-6} tolerance.

Tab. 6 shows the fault location errors resulting from each optimization algorithm, indicating mean errors, maximum absolute errors, and the standard deviations for each fault type. The investigation used the same fault as applied to the previously mentioned sensitivity analysis. It can be seen from Tab. 6 indicates that the DDEOPT solver yields fault location estimates with the lowest errors, corroborating the analysis of optimization solvers, as indicated in Section III-F.

TABLE 6. Fault distance errors in (%) considering different optimization solvers. Faults at 50% (128 [km]) from L terminal, resistance combination 5 (5;50), and phasors extracted from transient measurements (fault inception of 0.2791 [s]).

Fault type	Error metric	Differential evolution	Pattern search	Simulated annealing	Genetic algorithm
AG	**Mean**	-0.393	-9.947	-6.962	-14.855
	Std. dev.	0.034	14.61	14.65	17.880
	Max	0.440	38.59	31.90	45.273
BCG	**Mean**	0.007	0.087	-2.938	-1.354
	Std. dev.	0.004	1.706	9.242	2.811
	Max	0.015	3.302	15.88	7.973
BC	**Mean**	0.009	0.935	0.110	-2.792
	Std. dev.	0.004	1.889	8.782	2.286
	Max	0.020	3.414	17.30	5.368
ABCG	**Mean**	-0.527	0.654	-3.164	3.361
	Std. dev.	0.279	14.02	6.776	11.689
	Max	0.836	40.38	17.36	26.773

V. CONCLUSION

Within the context of power transmission over large distances, the use of series compensation in the lines is beneficial, as it increases the power flow capacity and improves the power system's stability. However, the non-linear behavior of series compensators adversely affects fault location algorithms on compensated lines. Therefore, this paper presented an algorithm for locating faults in series-compensated lines to remedy deficiencies found in the literature review.

From the resolution of a minimization problem, which considers the measured and calculated post-fault phasors and for which the DDEOPT solver proved superior over other optimization solvers, the proposed algorithm can locate faults with precision and robustness, even in critical cases with errors in the parameters of the considered line and the phasors extraction. As an important achieved objective, the proposed method was able to locate the fault even in critical cases faced by existing methods. The objectives reached by the method were: no need for measurements obtained after the SC bypass and knowledge regarding the MOV's operation point and impedance. In addition, the algorithm is applicable for every fault type and it is not affected by the SC positioning.

The results emphasize that the method succeeded in meeting all the established objectives. It can satisfactorily locate any type of fault, regardless of the fault's distance and resistance. As a worst case scenario in the precision analysis, the fault location error using transient data was around 1%.

REFERENCES

[1] P. Kundur, *Power System Stability and Control*. New York, NY, USA: McGraw-Hill, 1994.

[2] L. Kilgore, L. Elliott, and E. Taylor, "The prediction and control of self-excited oscillations due to series capacitors in power systems," *IEEE Trans. Power App. Syst.*, vol. PAS-90, no. 3, pp. 1305–1311, May 1971.

[3] R. Rajarman, F. Alvarado, A. Maniaci, R. Camfield, and S. Jalali, "Determination of location and amount of series compensation to increase power transfer capability," *IEEE Trans. Power Syst.*, vol. 13, no. 2, pp. 294–300, May 1998.

[4] D. Korot, P. Marken, and L. Bock, "The next fifty years of series capacitors and the last eighty-six," in *Proc. IEEE PES T&D Conf. Exp.*, Apr. 2014, pp. 1–5.

[5] J. Lakkireddy, R. Rastgoufard, I. Leevongwat, and P. Rastgoufard, "Steady state voltage stability enhancement using shunt and series FACTS devices," in *Proc. Clemson Univ. Power Syst. Conf.*, Mar. 2015, pp. 1–5.

[6] C. A. Ordóñez, A. Gómez-Expósito, and J. M. Maza-Ortega, "Series compensation of transmission systems: A literature survey," *Energies*, vol. 14, no. 6, p. 1717, Mar. 2021.

[7] Y. Zhang, J. Liang, Z. Yun, and X. Dong, "A new fault-location algorithm for series-compensated double-circuit transmission lines based on the distributed parameter model," *IEEE Trans. Power Del.*, vol. 32, no. 6, pp. 2398–2407, Nov. 2017.

[8] T. P. S. Bains, T. S. Sidhu, Z. Xu, I. Voloh, and M. R. D. Zadeh, "Impedance-based fault location algorithm for ground faults in series-capacitor-compensated transmission lines," *IEEE Trans. Power Del.*, vol. 33, no. 1, pp. 189–199, Feb. 2018.

[9] M. Saha, J. Izykowski, E. Rosolowski, and B. Kasztenny, "A new accurate fault locating algorithm for series-compensated lines," *IEEE Trans. Power Del.*, vol. 14, no. 3, pp. 789–797, Jul. 1999.

[10] M. M. Saha, K. Wikstrom, J. Izykowski, and E. Rosolowski, "Fault location in uncompensated and series-compensated parallel lines," in *Proc. IEEE Power Eng. Soc. Winter Meeting. Conf.*, Jan. 2000, pp. 2431–2436.

[11] C.-S. Yu, C.-W. Liu, S.-L. Yu, and J.-A. Jiang, "A new PMU-based fault location algorithm for series-compensated lines," *IEEE Trans. Power Del.*, vol. 17, no. 1, pp. 33–46, Aug. 2002.

[12] J. Izykowski, E. Rosolowski, P. Balcerek, M. Fulczyk, and M. M. Saha, "Fault location on double-circuit series-compensated lines using two-end unsynchronized measurements," *IEEE Trans. Power Del.*, vol. 26, no. 4, pp. 2072–2080, Oct. 2011.

[13] S. Hussain and A. Osman, "Fault location on series-compensated lines using unsynchronized measurements," in *Proc. IEEE Power Energy Soc. Gen. Meeting*, Jul. 2013, pp. 1–5.

[14] N. Kang, J. Chen, and Y. Liao, "A fault-location algorithm for series-compensated double-circuit transmission lines using the distributed parameter line model," *IEEE Trans. Power Del.*, vol. 30, no. 1, pp. 360–367, Feb. 2015.

[15] Y. Deng, Z. He, R. Mai, S. Lin, and L. Fu, "Fault location estimator for series compensated transmission line under power oscillation conditions," *IET Gener., Transmiss. Distrib.*, vol. 10, no. 13, pp. 3135–3141, Oct. 2016.

[16] T. P. S. Bains and M. R. D. Zadeh, "Supplementary impedance-based fault-location algorithm for series-compensated lines," *IEEE Trans. Power Del.*, vol. 31, no. 1, pp. 334–342, Feb. 2016.

[17] S. Gajare and A. K. Pradhan, "An accurate fault location method for multi-circuit series-compensated transmission lines," *IEEE Trans. Power Syst.*, vol. 32, no. 1, pp. 572–580, Jan. 2016.

[18] M. Nemati, M. Bigdeli, A. Ghorbani, and H. Mehrjerdi, "Accurate fault location element for series compensated double-circuit transmission lines utilizing negative-sequence phasors," *Electr. Power Syst. Res.*, vol. 194, May 2021, Art. no. 107064.

[19] A. Saffarian and M. Abasi, "Fault location in series capacitor compensated three-terminal transmission lines based on the analysis of voltage and current phasor equations and asynchronous data transfer," *Electr. Power Syst. Res.*, vol. 187, Oct. 2020, Art. no. 106457.

[20] R. Taheri, M. Eslami, and Y. Damchi, "Single-end current-based algorithm for fault location in series capacitor compensated transmission lines," *Int. J. Electr. Power Energy Syst.*, vol. 123, Dec. 2020, Art. no. 106254.

[21] J. Sadeh, N. Hadjsaid, A. Ranjbar, and R. Feuillet, "Accurate fault location algorithm for series-compensated transmission lines," *IEEE Trans. Power Del.*, vol. 15, no. 3, pp. 1027–1033, Jul. 2000.

[22] J. Sadeh and A. Adinehzadeh, "Accurate fault location algorithm for transmission line in the presence of series connected FACTS devices," *Int. J. Electr. Power Energy Syst.*, vol. 32, no. 4, pp. 323–328, May 2010.

[23] M. Ghazizadeh-Ahsaee, "Time-domain based fault location for series compensated transmission lines without requiring fault type," *Electric Power Syst. Res.*, vol. 181, Apr. 2020, Art. no. 106171.

[24] Z. Huang, Y. Chen, and Q. Gong, "A protection and fault location scheme for EHV line with series capacitor based on travelling waves and wavelet analysis," in *Proc. Int. Conf. Power Syst. Technol.*, Oct. 2002, pp. 290–294.

[25] M. Abedini, A. Hasani, A. H. Hajbabaie, and V. Khaligh, "A new traveling wave fault location algorithm in series compensated transmission line," in *Proc. 21st Iranian Conf. Electr. Eng. (ICEE)*, May 2013, pp. 1–6.

[26] B. Sahoo and S. R. Samantaray, "An enhanced fault detection and location estimation method for TCSC compensated line connecting wind farm," *Int. J. Electr. Power Energy Syst.*, vol. 96, pp. 432–441, Mar. 2018.

[27] O. D. Naidu and A. K. Pradhan, "Model free traveling wave based fault location method for series compensated transmission line," *IEEE Access*, vol. 8, pp. 193128–193137, 2020.

[28] G. Manassero, S. G. Di Santo, and L. Souto, "Heuristic method for fault location in distribution feeders with the presence of distributed generation," *IEEE Trans. Smart Grid*, vol. 8, no. 6, pp. 2849–2858, Aug. 2016.

[29] D. Cai and J. Zhang, "New fault-location algorithm for series-compensated double-circuit transmission line," *IEEE Access*, vol. 8, pp. 210685–210694, 2020.

[30] G. Manassero Junior, S. G. Di Santo, and D. G. Rojas, "Fault location in series-compensated transmission lines based on heuristic method," *Electr. Power Syst. Res.*, vol. 140, pp. 950–957, Nov. 2016.

[31] M. T. Hoq, J. Wang, and N. Taylor, "An incremental quantity based distance protection with capacitor voltage estimation for series compensated transmission lines," *IEEE Access*, vol. 9, pp. 164493–164502, 2021.

[32] H. Li, M. Abdeen, Z. Chai, S. Kamel, X. Xie, Y. Hu, and K. Wang, "An improved fast detection method on subsynchronous resonance in a wind power system with a series compensated transmission line," *IEEE Access*, vol. 7, pp. 61512–61522, 2019.

[33] T. P. S. Bains and M. R. D. Zadeh, "Enhanced phasor estimation technique for fault location in series-compensated lines," *IEEE Trans. Power Del.*, vol. 30, no. 4, pp. 2058–2060, Aug. 2015.

[34] J. F. Hauer, C. J. Demeure, and L. L. Scharf, "Initial results in Prony analysis of power system response signals," *IEEE Trans. Power Syst.*, vol. 5, no. 1, pp. 80–89, Feb. 1990.

[35] J. Grainger and W. Stevenson, *Power System Analysis*. New York, NY, USA: McGraw-Hill, 1994.

[36] W. I. Bowman and J. M. McNamee, "Development of equivalent pi and t matrix circuits for long untransposed transmission lines," *IEEE Trans. Power App. Syst.*, vol. PAS-83, no. 6, pp. 625–632, Jun. 1964.

[37] D. L. Goldsworthy, "A linearized model for mov-protected series capacitors," *IEEE Trans. Power Syst.*, vol. PS-2, no. 4, pp. 953–957, Nov. 1987.

[38] R. Storn and K. Price, "Differential evolution—A simple and efficient heuristic for global optimization over continuous spaces," *J. Global Optim.*, vol. 11, no. 4, pp. 341–359, 1997.

[39] A. Qing, "Dynamic differential evolution strategy and applications in electromagnetic inverse scattering problems," *IEEE Trans. Geosci. Remote Sens.*, vol. 44, no. 1, pp. 116–125, Jan. 2006.

[40] L. Ingber and B. Rosen, "Genetic algorithms and very fast simulated reannealing: A comparison," *Math. Comput. Model.*, vol. 16, no. 11, pp. 87–100, Nov. 1992.

[41] *IEEE Standard for Synchrophasor Measurements for Power Systems*, Standard C37.118.1-2011, 2011, pp. 1–61.

SILVIO GIUSEPPE DI SANTO was born in Brazil, in 1983. He received the B.Sc. degree from Universidade Estadual Paulista (UNESP), in 2007, and the M.Sc. and Ph.D. degrees from the Universidade de São Paulo (USP), in 2010 and 2013, respectively. Since 2013, he has been an Assistant Professor at USP. He is currently working on three projects, such as substation 4.0: a study of requirements and performance of a protection system, control, automation and monitoring, energy and automation and integrated storage system to more than one energy source.

ALVARO DA ROCHA ALBERTINI was born in Brazil, in 1995. He received the B.Sc. and M.Sc. degrees in electrical engineering from a double degree program between the Universidade de São Paulo, Brazil, and the Technische Universität Darmstadt, Germany, in 2021. He is currently pursuing the M.Sc. degree with the University of São Paulo, research focused on the impacts of distributed generation management systems and the provision of grid services from DERs.

RODRIGO ROZENBLIT TIFERES was born in Brazil, in 1998. He received the B.Sc. degree from the Universidade de São Paulo (USP), São Paulo, Brazil, in 2020, where he is currently pursuing the M.Sc. degree in electrical and power engineering. His research interests include power systems protection, modeling, and simulation.

• • •